

# Thermal fronts and cross-frontal heat flux in the southern Huanghai Sea and the East China Sea

PARK Sunghyea<sup>1\*</sup>, CHU Peter C<sup>1</sup>

1. Department of Oceanography, Naval Postgraduate School, Monterey, CA93943, USA

Received 31 August 2007; accepted 4 March 2008

## Abstract

Synoptic features in/around thermal fronts and cross-frontal heat fluxes in the southern Huanghai/Yellow Sea and East China Sea (HES) were examined using the data collected from four airborne expendable bathythermograph surveys with horizontal approximately 35 km and vertical 1 m (from the surface to 400 m deep) spacings. Since the fronts are strongly affected by HES current system, the synoptic thermal features in/around them represent the interaction of currents with surrounding water masses. These features can not be obtained from climatological data. The identified thermal features are listed as follows: (1) multiple boundaries of cold water, asymmetric thermocline intrusion, locally-split front by homogeneous water of approximately 18 °C, and mergence of the front by the Taiwan Warm Current in/around summertime southern Cheju – Changjiang/Yangtze front and Tsushima front; (2) springtime frontal eddy-like feature around Tsushima front; (3) year-round cyclonic meandering and summertime temperature-inversion at the bottom of the surface mixed layer in Cheju – Tsushima front; and (4) multistructure of Kuroshio front. In the Kuroshio front the mean variance of vertical temperature gradient is an order of degree smaller than that in other HES fronts. The southern Cheju – Changjiang front and Cheju – Tsushima front are connected with each other in the summer with comparable cross-frontal temperature gradient. However, cross-frontal heat flux and lateral eddy diffusivity are stronger in the southern Cheju – Changjiang front. The cross-frontal heat exchange is the largest in the mixing zone between the modified Huanghai Sea bottom cold water and the Tsushima Warm Current, which is attributable to enhanced thermocline intrusions.

**Key words:** southern Huanghai Sea and East China Sea, AXBT, synoptic thermal front, cross-frontal heat flux, lateral eddy diffusivity

## 1 Introduction

The Huanghai Sea and East China Sea (HES) are marginal seas of the western Pacific Ocean, bounded by China, Korea, and Japan in the west, north, and east, and reach the Okinawa Trench in the south (Fig. 1). With a border line connecting the Changjiang/Yangtze

River mouth and Cheju-do, north of HES is the Huanghai Sea (HS), and south the East China Sea (ECS). About 70% of YES is covered with a well-developed continental shelf of a depth shallower than 200 m, and the rest with a deep trench of steep bottom topography. Not only these geographical characteristics but also the Kuroshio intrusion from the south facilitates the occurrence of fronts.

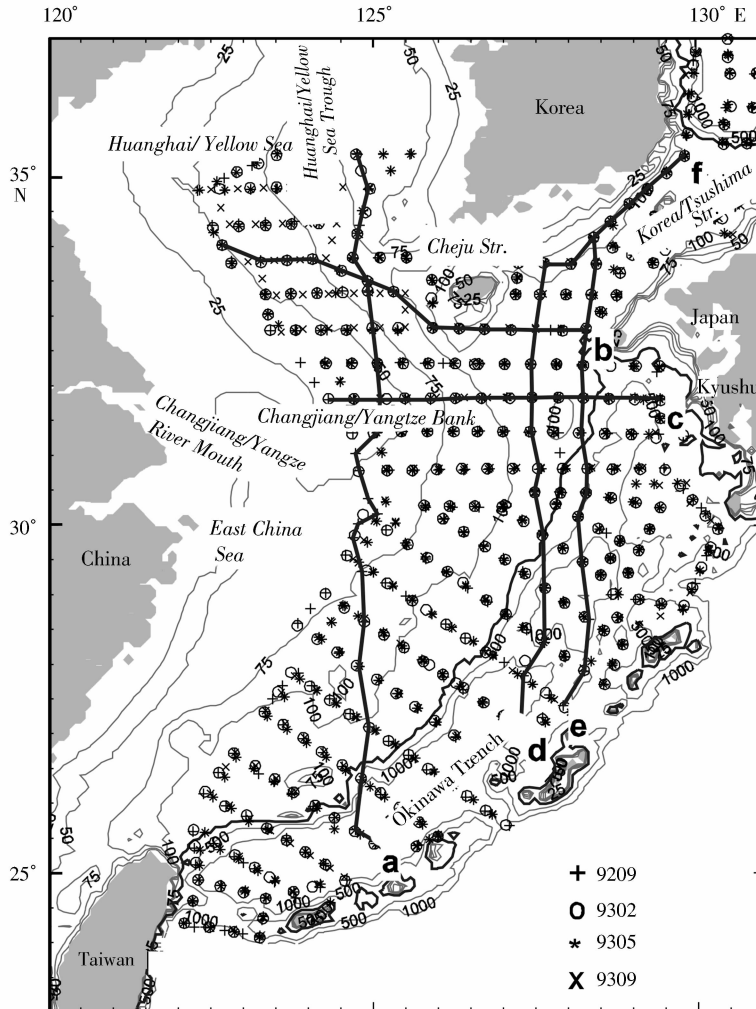


Fig. 1. Four airborne expendable bathythermograph (AXBT) surveys conducted on 18 ~ 29 September 1992 (9209), 4 ~ 14 February 1993 (9302), 5 ~ 14 May 1993 (9305) and 2 ~ 10 September 1993 (9309). Six sections (section-a through section-f) are used to describe the vertical temperature distributions. Contours indicate the bathymetry shallower than 1000 m, and the isobath of 200 m is highlighted by a thick black line.

The HS has large temporal and spatial thermal variability (Chu, Wells et al., 1997; Chu, Fralick et al., 1997). Surface thermal fronts throughout HES have been studied comprehensively using remotely-sensed data since the 1970s. Ning et al. (1998) identified five fronts derived from combined AVHRR SST and CZCS-derived pigment concentration data. Hickox et al. (2000) produced year-round climatology of ten thermal fronts based on Pathfinder

SST (1985 ~ 1996). It is however for specific regions that the studies including subsurface thermal frontal features have been done using in situ observations; for instance, along the Kuroshio (Chu et al., 2005; Yan et al., 2003; Oka and Kawabe, 1998; Hsu et al., 1997; Qui et al., 1990), along the Tsushima Warm Current (Lee et al., 2003; Guo et al., 1998), around the Huanghai/Yellow Sea Bottom Cold water (HSBCW) (Tang et al., 2000;

Hu, 1994), around the Cheju-do (Son et al., 2003), and along the southern coast of Korea (Kim and Yug, 1983). However, seldom have studies of subsurface thermal fronts throughout HES been done.

Recently, Park and Chu (2006b, hereafter PC06) identified the thermal and haline fronts at both surface and subsurface throughout HES from a climatological dataset [i. e., generalized digital Environmental model (GDEM)] with three-dimensional distributions and seasonality. Characteristics of the fronts were examined in terms of frontal intensity, water mass distribution, and temporal evolutions of temperature and salinity across the fronts. However, a variety of frontal features such as intrusion, inversion, and evidence of mixing could not be well presented because of inevitable weaknesses of the climatological dataset itself.

There were four airborne expendable bathythermograph (AXBT) surveys with horizontal spacing of 35 km and vertical resolution of 1 m from the surface to 400 m depth, which are invaluable to explore synoptic thermal features throughout the southern HS, the ECS, and the southern Japan/East Sea at both surface and subsurface. For HES these surveys cover the region from the deep trench to the shelf as shallow as 50 ~ 75 m depth (Fig. 1). Using these AXBT data, Furey and Bower (2005, hereafter FB05) analyzed variability of mixed layer depth, path change of the Kuroshio associated with generation of cold eddies on canyons northeast off Taiwan, and seasonal evolution of thermal fronts in the HES and the Japan/East Sea. Park and Chu (2008, 2007) examined characteristics of HES finestructures in temperature profiles, their generation mechanisms, related mixing processes, synoptic features of vertical layers, and the Monin-Obukhov depth.

As a companion of their studies, we explore detail synoptic features in/around thermal fronts in

the HES, which have not been reported in other studies. These data reveal various synoptic thermal features in/around the fronts; for instance, inversions (temperature increases with depth), multilayers (a temperature profile is vertically fluctuated and then is divided into several layers such as a temperature-inverted layer, an isothermal layer, and so forth), and ragged isotherms (isotherms are “ragged”, not smooth, at a vertical scale of few to tens meters) are prominent in/around a front detected in 127.5°E (Fig. 2). However, these features are not seen in the climatological dataset (e. g., GDEM) at all even though the front is seen in 127.5°E. These synoptic thermal features, like an example in Fig. 2, can reveal how currents interact with surrounding water masses in/around the fronts since the fronts are strongly affected by the HES current system comprising the Kuroshio, the Tsushima Warm Current, the Taiwan Warm Current, and the Cheju Warm Current. In addition, we estimate cross-frontal heat flux and lateral eddy diffusivity in the fronts. Estimates of cross-frontal heat flux can quantify the front-contributed heat exchange with surrounding water masses, which is associated with frontal mixing. The estimates from observation data are useful for validating estimates from numerical simulations. In the HES where the fronts are dynamically related to each other by the connected current system, comparison of the cross-frontal heat flux among the fronts can predict the heat loss from the connected current system (only by cross-frontal heat exchange).

The rest of the paper is organized as follows. Section 2 gives a brief description of the AXBT data. Section 3 summaries how to identify the thermal fronts in the data. Section 4 describes the synoptic characteristics of the fronts with their horizontal/vertical distributions and presents plausible explanations on the frontal features in connection with the frontal structures, the water masses, and the circulation system. Section 5 estimates the cross-frontal

heat flux and the lateral eddy diffusivity. Section 6

presents conclusion.

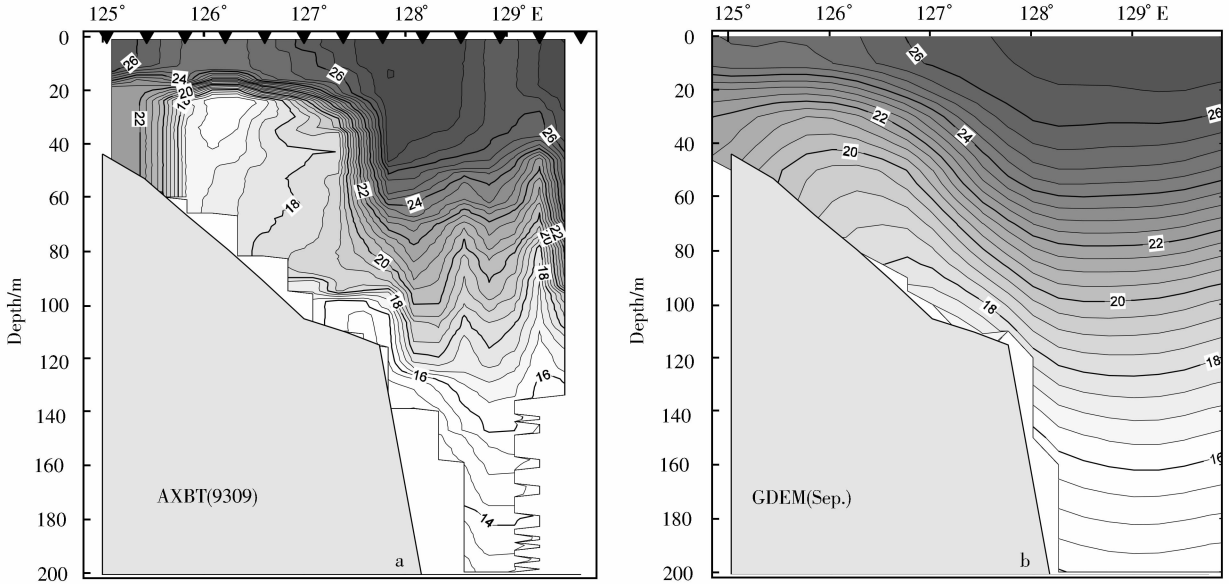


Fig. 2. Comparison of vertical temperature distributions along 31.3°N between AXBT (a) and GDEM (b). Downward pointing triangles mark locations of AXBT deployments.

## 2 AXBT measurements

The AXBT data consist of 1256 profiles from the four surveys (Fig. 1): 18 ~ 29 September 1992 (named as 9209), 4 ~ 14 February 1993 (as 9302), 5 ~ 14 May 1993 (as 9305), and 2 ~ 10 September 1993 (as 9309). The data, a part of the Master Oceanographic Observation Data Set (MOODS), were obtained under the approval by the Naval Oceanographic Office (NAVOCEANO). The data including their detail information have not been open to the public yet. In the 1990s, Sparton AXBTs were widely used in U.S. Navy research. Their thermal time constant 0.1 s or less and their vertical resolution is 15 cm (Boyd and Linzell, 1993). We obtained the edited AXBT data with 1 m vertical resolution. The editing process includes the followings: identifying recording errors and outliers, checking duplicate profiles, checking depth inversion and depth duplication for individual profiles, checking temperature range, checking large temperature in-

versions and gradients, checking standard deviation, interpolation to standard levels, and post objective analysis checks (Chu et al., 1998; Chu, Fralick et al., 1997; Boyer and Levitus, 1994; Jugan and Beresford, 1992). Customized equations, which were achieved using concurrent CTD data, provide the accuracy of temperature data of 0.13°C and that of depth of  $\pm 2\%$  of depth or  $\pm 10$  m, whichever is greater. The Naval Research Laboratory (NRL) Isis System determines the AXBT frequency to such accuracy that the resulting temperature accuracy is 0.05°C or better (Boyd and Linzell, 1993).

The four surveys almost repeated themselves in track paths with slight mismatch and were completed within one week except for some profiles near the Korea/Tsushima Strait, so that the seasonality of the thermal features in/around the fronts can be identified. The synoptic variability of the thermal features can be identified only for the features with horizontal scales larger than tens kilometer and duration longer than a week.

### 3 Identification of fronts

A horizontal temperature gradient is expressed by

$$\Delta T(i) = \sqrt{\left(\frac{\partial T(i)}{\partial x}\right)^2 + \left(\frac{\partial T(i)}{\partial y}\right)^2},$$

where  $T(i)$  and  $i$  are temperature and spatial index, respectively (PC06). The gradient is calculated at 0 (the sea surface), 25, 50, and 75 m depths (Fig. 3). A thermal front is identified by the horizontal temperature gradient of greater than  $5^\circ\text{C}/100$  km, which is close to a criterion ( $2^\circ\text{C}/35$  km) applied by FB05 (see their Fig. 5 for the front schematic at 60 m depth) but greater than a criterion ( $2^\circ\text{C}/100$  km) by PC06 because fronts are usually sharper and stronger in in-situ observation than in the climatological dataset (as seen in Fig. 2). The gradient method is also used for satellite data; for instance,  $0.50^\circ\text{C}/9$  km for thermal fronts in the northern South China Sea using NOAA/NASA Pathfinder SST (Wang et al., 2001). The identified thermal fronts are Cheju Changjiang front (CCF), Cheju Tsushima front (CTF), Tsushima front (TF), and Kuroshio front (KF) (Fig. 3); their name and definition are referred to PC06. Their alternative names are in Hickox et al. (2000, Fig. 2). FB05 also presented a schematic of fronts at 60 m depth in their Fig. 6. CCF is two-tongue-shaped, northern and southern tongues. CTF occurs along the southern coast of Korea and expands between the Cheju Strait and the Korea/Tsushima Strait. TF is a branch from KF. The southern tongue of CCF migrates southward/southeastward from the winter to the summer (FB05; PC06). In warm seasons the southern tongue of CCF merges to TF and forms one broad front. In comparison with a map of the fronts of the climatological data (PC06, Fig. 5), the fronts show more spatial variability. Many minor front-like features unseen in the climatological data are located near the four major fronts, which will be explored in this study.

In addition to the horizontal temperature gradient distribution, we will show horizontal temperature distributions at 25 and 50 m depths and vertical ones along Section-a through Section-f to describe the fronts and related thermal features. The distribution at 25 m depth is suitable to show summertime thermal features induced by bottom cold waters on the shallow shelf. Its February distribution shows the all major thermal fronts in single plot (see the fronts drawn in Figs 3 and 4). The distribution at 50 m depth has been frequently seen in many studies to show hydrographic features near the bottom in HES (Lie et al., 2000; Isobe, 1999; Park, 1986), so that it can be conveniently compared with others although it is similar to the distribution at 60 m (FB05, Fig. 4). See FB05 for more horizontal temperature distributions (at 60 and 100 m depths) and vertical ones (on ECS shelf and Cheju-do to the Korea/Tsushima Strait).

### 4 Synoptic features of the fronts

#### 4.1 Cold water masses in the southern CCF tongue

In the winter the southern tongue of CCF is viewed as the southward/southeastward invasion of the cold water (9302 in Figs 4 and 5). A single cold water mass exists over  $29.5^\circ \sim 32.5^\circ$  N with the central temperature of less than  $10^\circ\text{C}$  (9302 in Fig. 6). From the winter to the spring, the sharp front still exists below 20 m depth [see isotherms of  $13^\circ \sim 16^\circ\text{C}$  around  $30^\circ$  N (9302, and 9305 in Fig. 4)] and is shifted southeastward (9302, 9305 in Fig. 4). Multiple cold water masses are generated in the spring and last in the summer with temperature of less than  $10^\circ\text{C}$  (HSBCW),  $10^\circ \sim 12.5^\circ\text{C}$ , and  $13^\circ \sim 15^\circ\text{C}$  (9305, 9209 and 9309 in Figs 6 and 7); the last two cold water masses are mixed water (named as modified HSBCW). The modified YSBCW

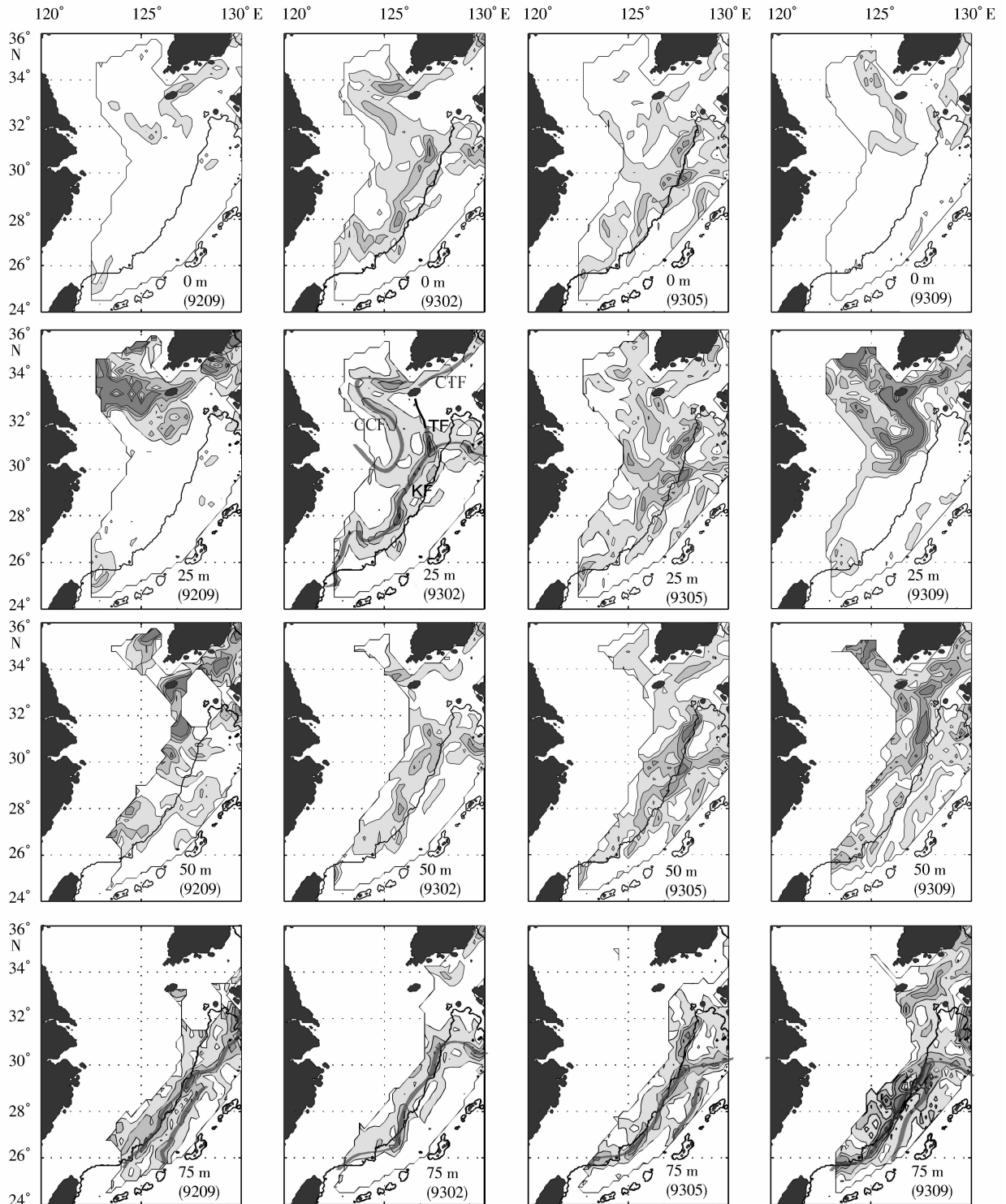


Fig. 3. Horizontal distributions of temperature gradient at 0, 25, 50, 75 m depths. Contour interval is  $2.5^{\circ}\text{C}/100\text{ km}$  and the contour of greater than  $10^{\circ}\text{C}/100\text{ km}$  is omitted. Considered the horizontal temperature distribution as well (Fig. 4), fronts such as Cheju-Changjiang Front (CCF), Cheju-Tsushima front (CTF), Tsushima front (TF), and Kuroshio front (KF) are depicted by thick grey lines in 19302 – 25 m. A part of TF, where the gradient is not as strong as  $2.5^{\circ}\text{C}/100\text{ km}$  but TF is thought to be, is marked darker. The distribution at 75 m shows a multi-structure of KF by the thick grey lines (see Section 4.9). The isobath of 200 m is highlighted by the thick black line.

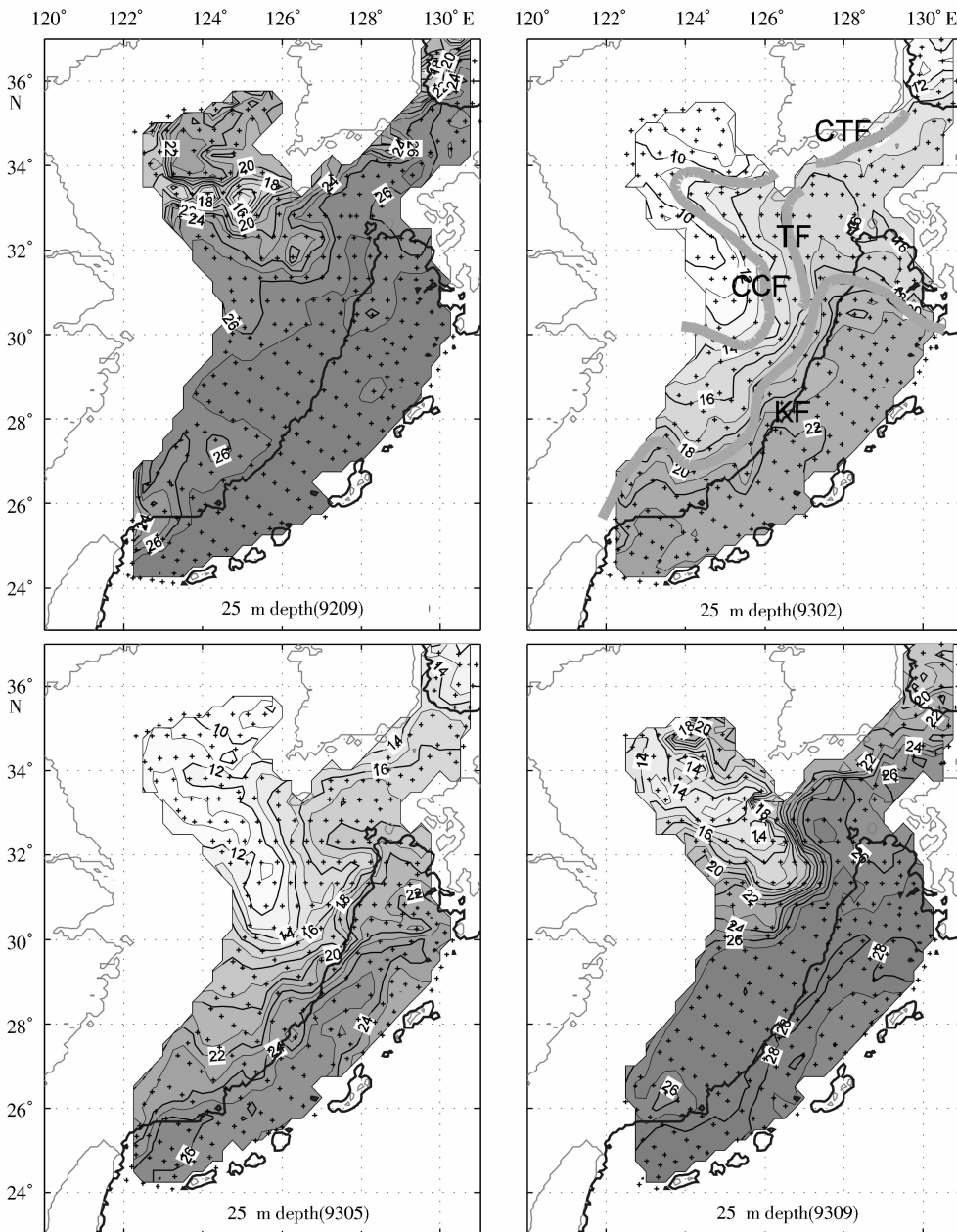


Fig. 4. Horizontal temperature distributions at 25 m depth showing the fronts. The isobath of 200 m is highlighted by a thick black line. Crosses mark locations of AXBT deployments.

is affected by surface heating, horizontal advection, and degree of mixing, resulting in seasonal change in its volume and location. It is also detected in several studies (Isobe, 1999; Chen et al., 1994; Park, 1986; FB05 (with same data)) with temperature ranging slightly different from this study though.

#### 4.2 Year-to-year variability in the summer CCF and TF

In the summer the northern CCF tongue weakens, and TF strengthens. The southern CCF tongue connects to CTF at the subsurface instead (FB05 (with same data); PC06). In 9209, isotherms mean-

der with strong temperature gradient from the eastern tip of the Changjiang/Yangtze Bank to the Korea/Tsushima Strait (9209 in Fig. 5). Compared with the climatology (PC06), the southern CCF tongue is shifted northward and 3 ~ 5°C warmer in the southern HS trough and the Changjiang Bank (9209 in Fig. 4). In 9309, on the other hand, isotherms meander less with moderate gradient and 2 ~ 3°C colder than the climatology, and the southern CCF tongue extends farther southeastward (9309 in Figs 4 and 5). These contrast features between the two summers are attributable to contrast atmospheric forcing, stronger wind in 1992 (weaker wind in 1993) than the normal (Yoo et al., 2004; Park and Chu, 2006a). According to COADS monthly wind data, stronger wind blows generally southwestward/westward in 9209 (Park and Chu, 2007). Consequently, more warm water invades northward by the Ekman transport, leading to thicker surface mixed layer. HSBCW shrinks toward the bottom, and the modified HSBCW does not extend farther southeastward.

#### 4.3 Mergence of thermal front by the Taiwan Warm Current in summer

In the summer two fronts are merged at 125° ~ 127°E and 30° ~ 31°N (9209 and 9309 in Figs 4 and 5). The northern one is the southern CCF describing a distinct boundary against the modified HSBCW, and the southern one is generated by the Taiwan Warm Current and/or the uplifted Kuroshio northeast off Taiwan according to its temperature range (23° ~ 27°C) (Hur et al., 1999). This mergence of the southern front into the southern CCF supports that the Taiwan Warm Current is one of sources of the Tsushima Warm Current in the summer (Isobe, 1999; Ichikawa and Beardsley, 2002; also presented by FB05). As the volume transport of these warm waters increases from spring to summer, the volume of the mixed water between these warm waters and the cold shelf water increa-

ses. This mixed water, a relatively homogeneous water mass of 22° ~ 23°C, resides between the two fronts, generally along the shelf in both summers, but is detected at shallower depth in 9309 (9209 and 9309 in Figs 4 and 5; see 30° ~ 31°N in Fig. 6-9309).

#### 4.4 Asymmetric thermocline intrusion around the southern CCF tongue

Vertically homogenous structure around the southern tongue of CCF in the winter implies strong wind and/or convective mixing prevails over horizontal advection or mixing. In other seasons the isotherms are not vertically uniform around the tongue. Note ragged isotherms are more evident around the eastern side of the tongue (e. g., 127° ~ 127.5°E in Fig. 8-9209) than around the western side of the tongue (e. g., approximately 125.5°N in Fig. 8-9209). This vertical structure that temperature profiles display multilayered or inverted structures at thermocline depths is called thermocline intrusion (Ruddick and Richards, 2003). The western side of the tongue is located on the shallow bank where the bottom tidal mixing is strong, resulting in the lack of ragged isotherms around the tongue.

In the spring the ragged isotherms on the eastern side of the tongue exhibit high possibility of mixing (126° ~ 127°E in Fig. 8-9305). In the summer the isotherms in the upper part of the tongue is inclined seaward and shows rich-ragged structures (126° ~ 127°E in Fig. 8-9209 and 9309), which is attributable to seaward migration of the tongue. On the contrary, the isotherms in the lower part of the tongue intrude shoreward in relation to the mass compensation and/or the Tsushima Warm Current intrusion into the shelf region.

#### 4.5 Extrusion around the southern CCF tongue

The southern CCF tongue and TF are occasional-

ly combined or separated by variations of the colder water between the tongue and the Tsushima Warm Current. In 9209, the two fronts are combined, showing strong frontal intensity along 127°E (9209 in Fig. 5). In 9309, however, the two fronts are separated by relatively homogeneous water mass between the

fronts (126.5° ~ 127.5°E in Fig. 8 9309). In 9305 the fronts are separated as well (127.2° ~ 128.2°E in Fig. 8-9305). This separation may be caused by the extrusions of water from the southern tongue (see stars in Fig. 5). The two extrusion features represent different phenomena.

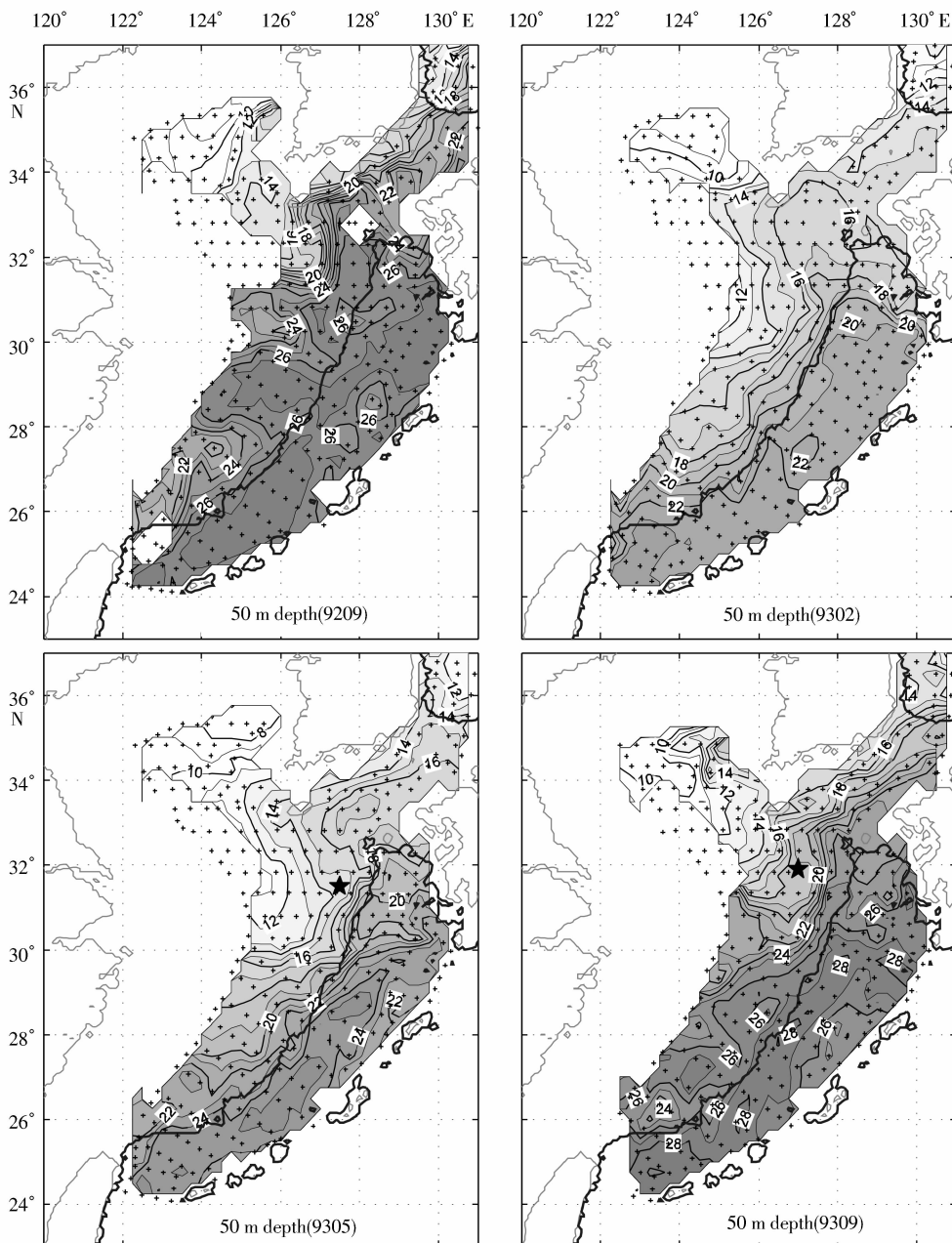


Fig. 5. Same as Fig. 4 except for 50 m depth. Temperature is shaded for the profiles extending to deeper 50 m depth. The star symbols are explained in the text.

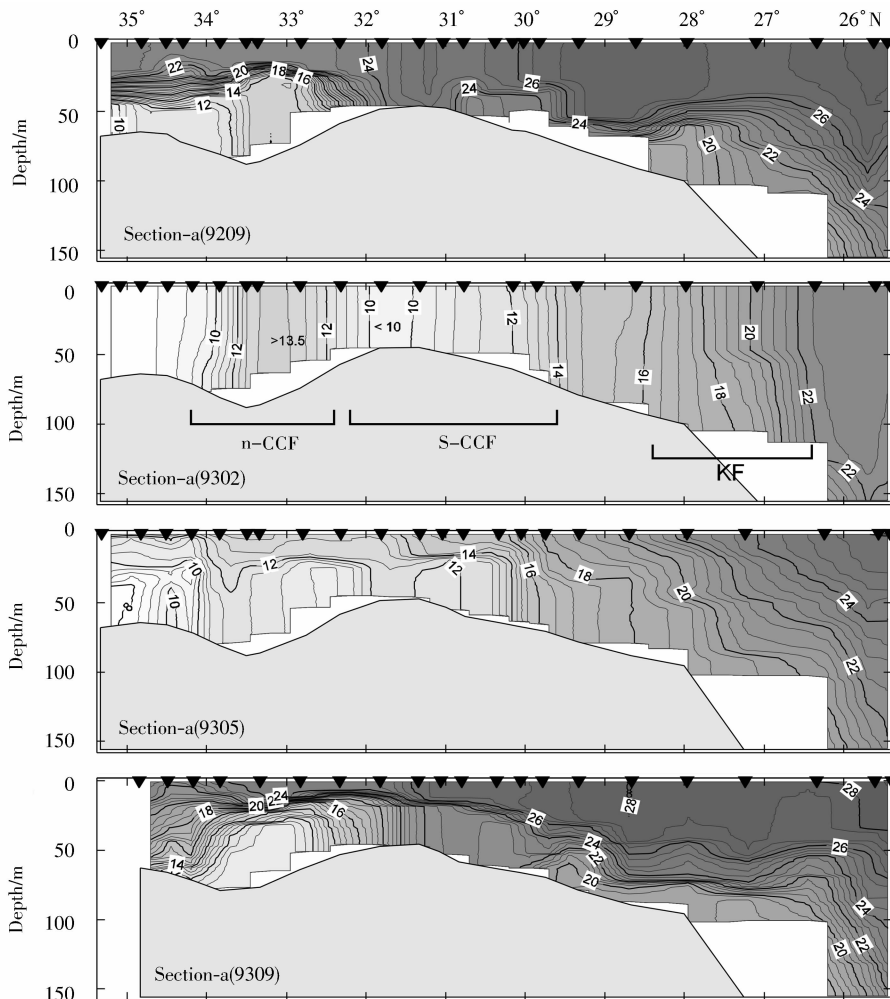


Fig. 6. Vertical temperature distributions along Section-a (see Fig. 1). Downward pointing triangles mark locations of AXBT deployments. The locations of northern tongue of CCF (n-CCF), southern tongue of CCF (S-CCF), and KF are marked with brackets.

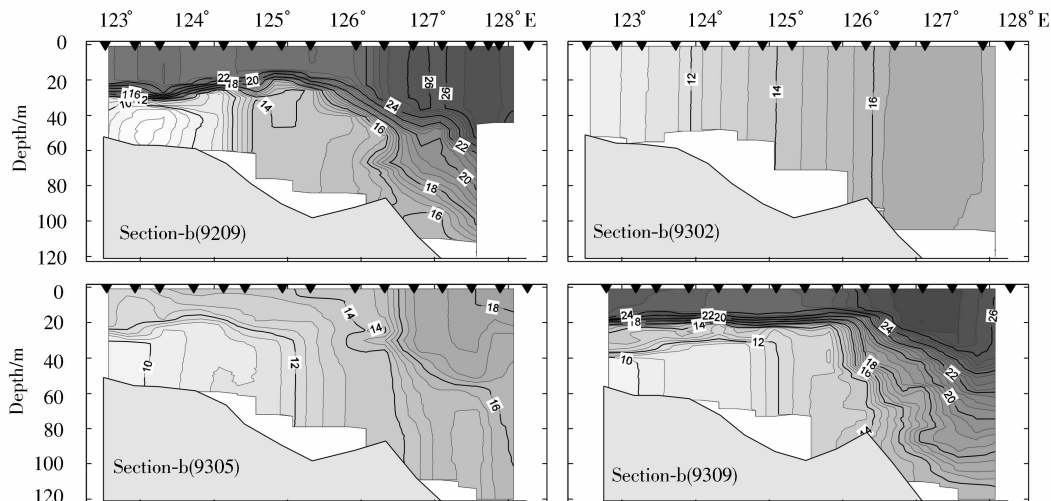


Fig. 7. Same as Fig. 6 except for section-b.

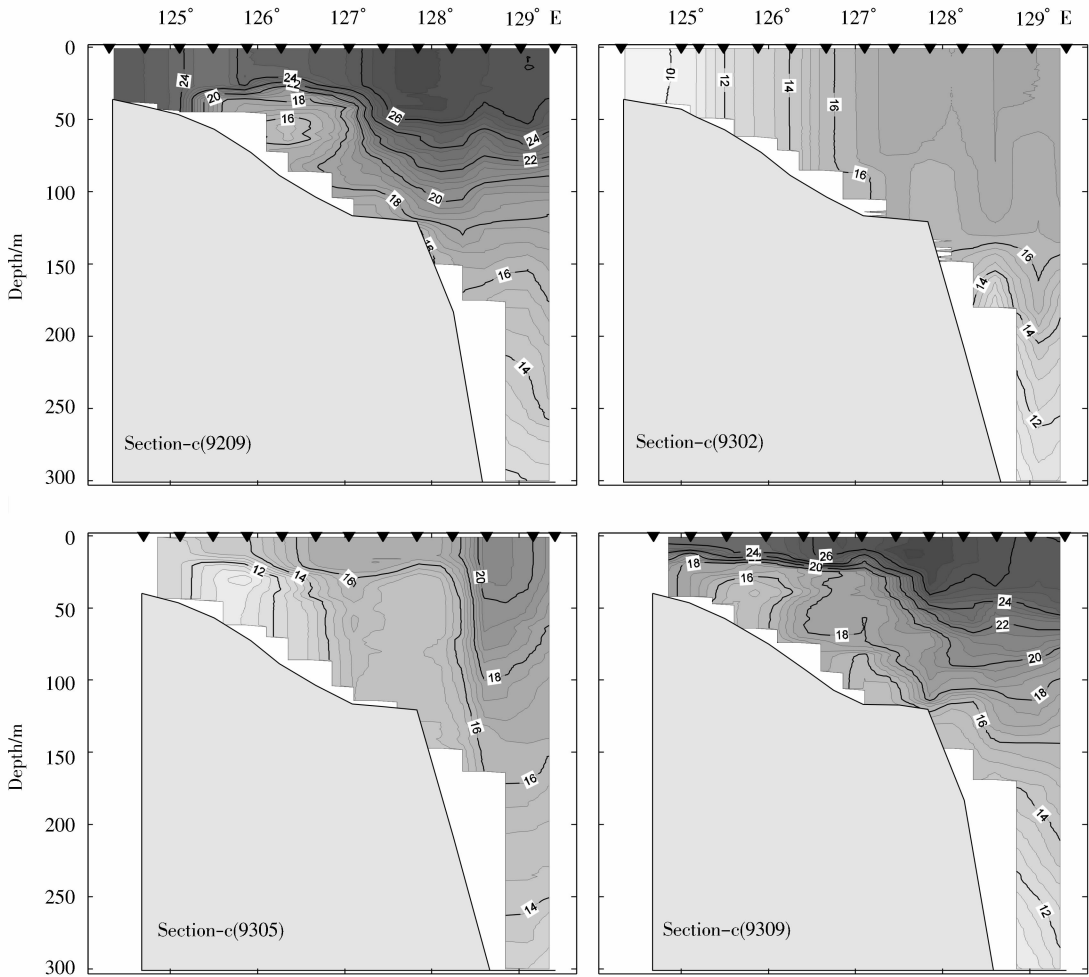


Fig. 8. Same as Fig. 6 except for section-c.

In 9309 the homogeneous water mass of around 18°C splitting locally the combined front of CCF and TF in a horizontal view ( Fig. 5-9309 ) is infiltrated into the thermocline in 127° ~ 128°E and eventually assimilated into neighboring thermocline( Fig. 8-9309 ). This feature looks like the vertical split of TF. The cross-section along 127.5°E shows that TF is split by the presence of the relatively homogenous water at 50 ~ 100 m depth (30.5° ~ 33°N in Fig. 9-9309 ). However, the cross-section along 128.2° E shows that this homogenous water is not distinguishable any more ( Fig. 10-9309 ). Meantime, the extrusion feature in 9305 might be associated with a frontal

eddy-like feature, which will be explained in Section 4.6.

#### 4.6 Frontal eddy-like feature around TF

In 9305 TF meanders cyclonically ( see the starin Fig. 5-9305 ), and thus upwelling can be induced in the center of this cyclonic meander. In Fig. 9-9305 cold water ( < 15°C ) is upwelled at 31.3° ~ 32°N, right before the shoreward boundary of TF(31°N; KF is in 29° ~ 30°N ), from the bottom to the near-surface on the shelf-break. This cold water is surrounded by warm water ( > 18°C ). These horizontal and vertical structures are similar to those of a frontal eddy, which is also seen in Fig. 8-9305

( $126.5^{\circ} \sim 128.5^{\circ}\text{E}$ ) and Fig. 10-9305 ( $31^{\circ} \sim 33^{\circ}\text{N}$ ). Fig. 4-9305 ( $127^{\circ} \sim 129^{\circ}\text{E}$ ,  $31^{\circ} \sim 33^{\circ}\text{N}$ ) also describes a frontal eddy-like feature with isotherms of  $18^{\circ} \sim 19^{\circ}\text{C}$ . Its horizontal scale is approximately 100 km, compatible to frontal eddies often detected around KF (Isobe et al., 2004; James et al., 1999;

Yanagi et al., 1998; Qui et al., 1990); however, a frontal eddy around TF has been seldom reported. Taking bottom topography and occurrence of a strong front (i. e., TF) into account, this region is appropriate to induce the frontal eddies as the Kuroshio region in the ECS.

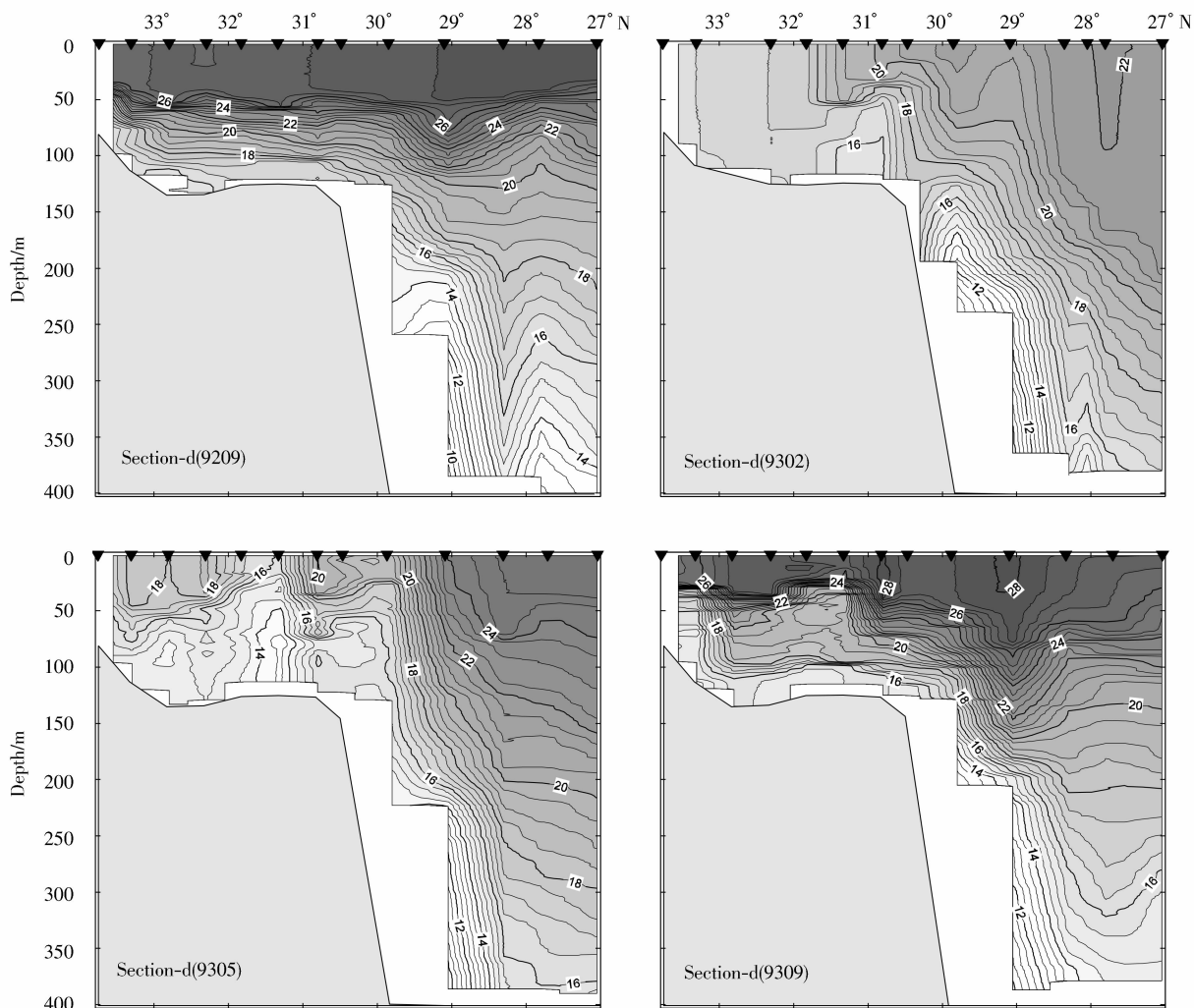


Fig. 9. Same as Fig. 6 except for section-d.

#### 4.7 Meandering of CTF

Year-round CTF is connected to either the northern (winter at all the depth) or the southern (summer at the subsurface) tongue of CCF/TF (PC06). CTF meanders more in the summer than in

the winter (Figs 4 and 5). A cyclonic meandering is marked around and  $34^{\circ} \sim 35^{\circ}\text{N}$   $128^{\circ} \sim 129^{\circ}\text{E}$  in 9209 (Figs 4 and 5). In the vertical view this cyclonic meandering is identified by a convex thermocline, which is above near-bottom cold water of  $14 \sim 16^{\circ}\text{C}$  ( $128.2^{\circ} \sim 129.2^{\circ}\text{E}$  in Fig. 11-9209). This

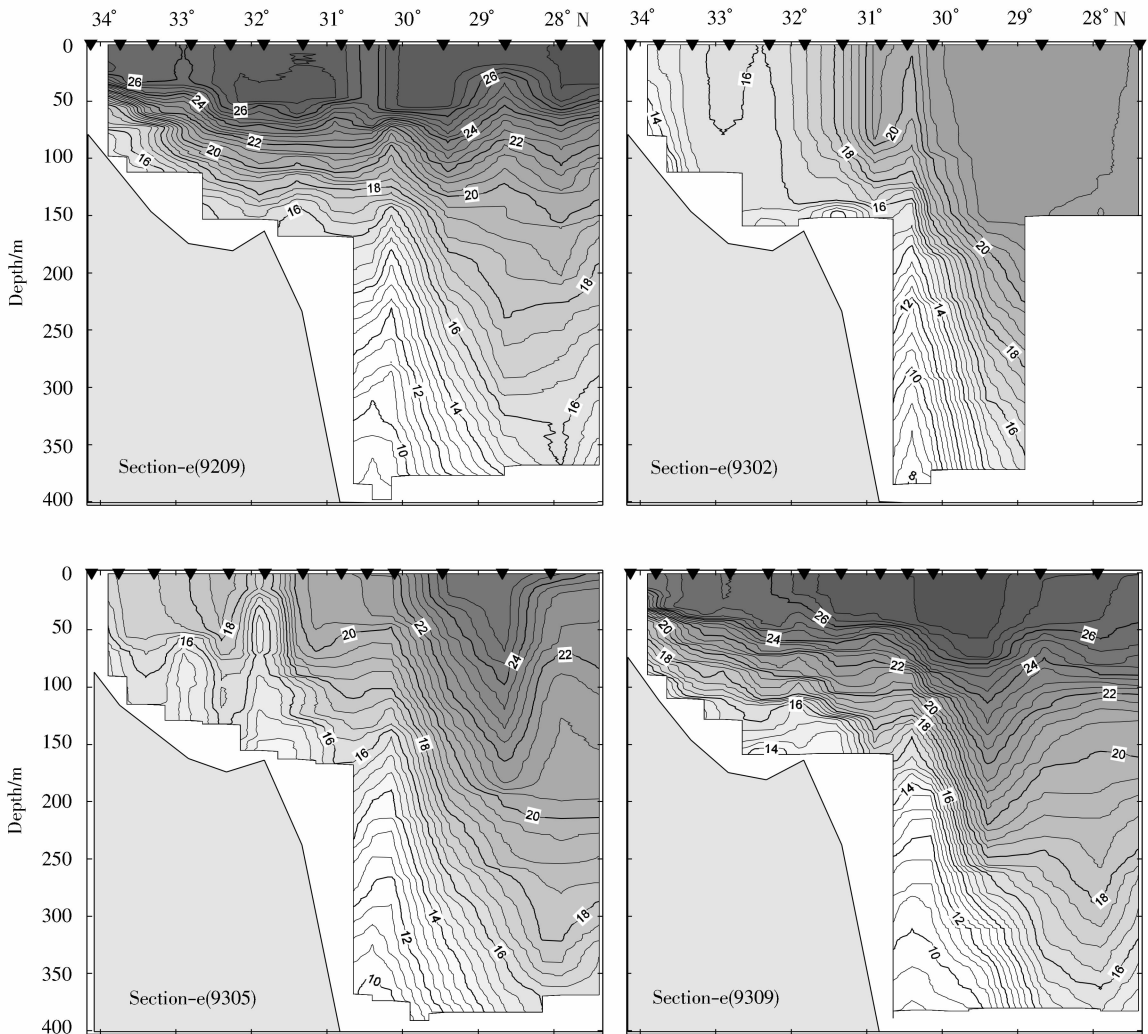


Fig. 10. Same as Fig. 6 except for section-e.

feature suggests that the cyclonic meandering is associated to the near-bottom cold water. The near-bottom cold water of approximately  $14^{\circ}\text{C}$  is also detected in the winter and spring (Fig. 11-9302 and 9305). Accordingly, the cyclonic meandering could be sustained throughout the season regardless of its spatio-temporal variability. The near-bottom cold water is expected to extend shoreward by Lee et al. (1984) observation, but its formation and maintaining mechanism are not known. In addition, it needs to be examined whether the near-bottom cold water induces the cyclonic meandering or vice versa.

#### 4.8 Warm-anomaly at the bottom of surface mixed layer in summer CTF

In both summers (9209 and 9309) temperature profiles in CTF show existence of warm-anomaly, i. e., inverted structures, describing that maximum temperature is observed between the surface mixed layer and the top of strong thermocline, at 10 ~ 50 m depth (see Fig. 3-9209 and 9309 in Park and Chu, 2008). The warm-anomaly is approximately 10 m thick and  $0.5^{\circ} \sim 1^{\circ}\text{C}$  warmer than surroundings. They are found in  $127.5^{\circ} \sim 128.5^{\circ}\text{E}$  and near  $129.5^{\circ}\text{E}$  along Section-f, where the isotherms are concave (9209 in Fig. 11). Such a shape of iso-

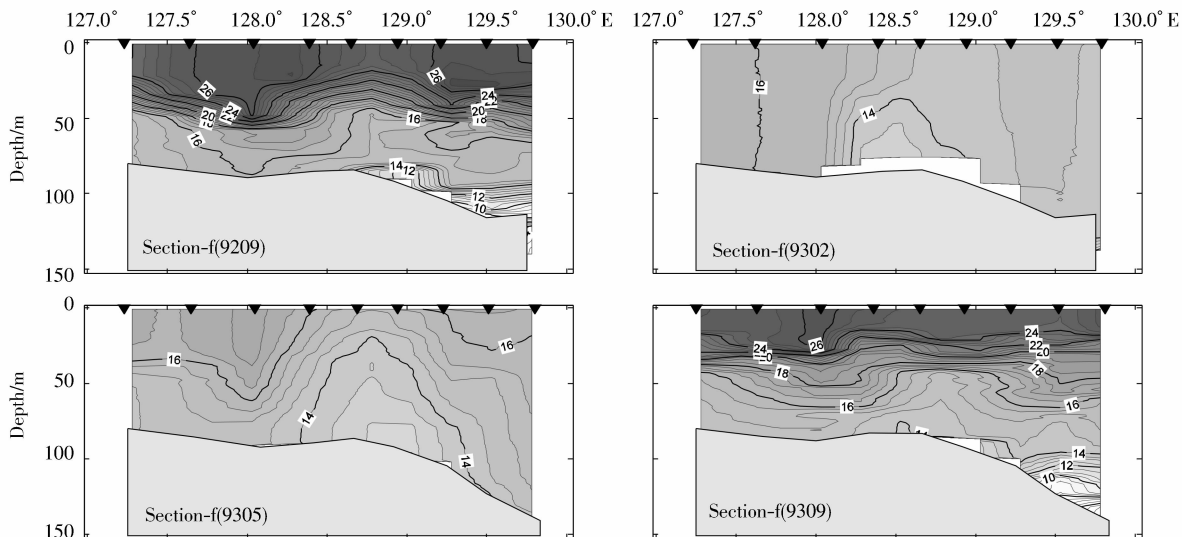


Fig. 11. Same as Fig. 6 except for section-f.

therms implies an anticyclonic motion, and downwelling is therefore possible there. The downwelling facilitates downward heat transfer. When stratification in thermocline is extremely strong, a part of downward heat flux does not transfer to the thermocline and thus piles up at the bottom of the surface mixed layer. The temperature near the bottom of the surface mixed layer therefore increases locally, yielding the inverted structure in the temperature profiles, i. e., the warm-anomaly. On the other hand, Kim and Yug (1983) reported a possibility of cold-water in the surface layer of this region in the summer, which might be caused by seaward movement of cold coastal water in the surface layer driven by summer monsoon (southwesterly). Since they presented neither temperature profiles nor a vertical resolution of the data, we cannot compare these inverted structures with theirs. In the AXBT data there is no evidence of the seaward movement of cold coastal water at upper 15 m depth in the region where the inverted structures are detected (not shown). Instead, an anticyclonic meandering of isotherms is found there. These inverted structures are plentiful in 9209 when the anticyclonic meandering

is strong (Figs 5 and 11; Fig. 3-9209 and 9309 in Park and Chu, 2008). What we explained above could be a possible scenario for these inverted structures although it is difficult to reach a firm conclusion at this moment without supportive observations.

#### 4.9 Multistructure of KF

In the summer the KF has a multistructure, i. e., inner/shoreward and outer/seaward KF, with warm eddies along the Okinawa Trench (see Fig. 6 in FB05, the horizontal temperature distribution at 100 m depth resembles that at 75 m depth); the horizontal temperature gradient distribution also confirms the multistructure (see grey thick lines in Fig. 3-75 m). The multistructure is depicted well, for instance, in Fig. 9-9309: the inner KF near 29.5°N, the warm eddy in near 29°N, and the outer KF in near 28.6°N. The inner KF following a 200 m isobath in Fig 3-75 m is the major one, which forms along the ECS shelf throughout the year. The outer KF, which is in the seaward of the inner KF and generally parallel to it, is most evident in the summer when the warm eddies grow. The outer KF is weaker and more distant from the inner KF in the

spring than in the summer. The outer KF is not detected in the winter. Since the outer KF is not as strong as the inner KF, it is hardly detected in the climatological data. Instead, a series of tongue-shaped isotherms represent the existence of warm eddies and the outer KF (PC06). The outer KF is interpreted as the southward return flow of the Kuroshio (Kondo, 1985) or a weak flow along the seaward boundary of the Kuroshio (FB05).

## 5 Cross-frontal heat flux

### 5.1 Joyce's model

A variability caused by intrusion or interleaving on scales of 1 ~ 100 m (finestructure) represents a source for smaller scale structure (microstructure) and a mechanism for cross-frontal heat/salt exchange; production of heat flux by cross-frontal advection (i. e., interleaving or intrusion) is balanced by destruction through intensive vertical mixing (Joyce, 1977). The thermocline intrusions often occur around the southern CCF tongue, TF, and CTF (Park and Chu, 2008). Also, haline intrusions might occur concurrently according to in situ observations (Lee et al., 2003; Bao et al., 1996). It is therefore possible to apply Joyce's model (1977) to estimate the cross-frontal heat flux.

The cross-frontal heat flux  $-\tilde{v}\tilde{T}$  and lateral eddy diffusivity  $\tilde{A}_T^H$  are expressed by

$$\left. \begin{aligned} -\tilde{v}\tilde{T} &= \overline{\tilde{A}_T^v \left( \frac{\partial \tilde{T}}{\partial z} \right)^2 \left/ \frac{\partial \tilde{T}}{\partial y} \right.} \\ \tilde{A}_T^H &= \overline{\tilde{A}_T^v \left( \frac{\partial \tilde{T}}{\partial z} \right)^2 \left/ \left( \frac{\partial \tilde{T}}{\partial y} \right)^2} \end{aligned} \right\} \quad (1)$$

where the tilde indicates finestructure-scale variables, and the overbar denotes averaging on scales larger than finestructure; i. e.,  $\tilde{v}$  and  $\tilde{T}$  are finestructure-scale velocity and temperature, respectively,  $\partial \tilde{T} / \partial y$  is horizontal cross-frontal temperature gradient

averaged over large-scale;  $(\partial \tilde{T} / \partial z)^2$  is variance of vertical finestructure-scale temperature gradient, and  $\tilde{A}_T^v$  is vertical Austausch coefficient for heat. Estimates for the vertical Austausch coefficient vary by two orders of magnitude, depending on mixing characteristics (Garrett, 1979). Since our knowledge of a precise value for the vertical Austausch coefficient is still incomplete, a constant value  $10^{-4} \text{ m}^2/\text{s}$  is assumed for it (Bao et al., 1996; Georgi, 1981; Joyce, 1977). The averaged variance of the vertical temperature gradient  $(\partial \tilde{T} / \partial z)^2$  is obtained by integrating temperature gradient spectrum from 4 to 40 m wavelength. The horizontal cross-frontal temperature gradient is measured using neighboring profiles in consideration for a direction of front.

Four parameters, i. e. the averaged variance of the vertical temperature gradient over depths, the cross-frontal temperature gradient, the cross-frontal heat flux, and the lateral eddy diffusivity, are listed in Tables 1 and 2. Table 1 shows averaged values over stations within grey boxes to compare the parameters among the HES fronts, while Table 2 shows values for individual stations marked by crosses to examine the parameters across or along a certain front (see Fig. 12 for their locations). If the thermocline intrusion or interleaving is not prominent in the profiles, the values remain blank in Tables 1 and 2.

### 5.2 Estimates of cross-frontal heat flux and lateral eddy diffusivity

In the summer the largest lateral eddy diffusivity exceeding  $O(10^2 \text{ m}^2/\text{s})$  is found south of Cheju, a mixing zone between the modified HSBCW and the Tsushima Warm Current water. The cross-frontal heat flux is also greatest, over  $O(10^{-2} \text{ }^\circ\text{C} \cdot \text{m}/\text{s})$ , there (south of Cheju-9209/9309 in Table 1). A sharp contrast between the two water masses and vertically-sheared advection (see Figs 7 and 8) might be responsible for large exchange of heat and probably salt. The summer

connected southern CCF/TF—south of Cheju—CTF have roughly equal, strong cross-frontal temperature gradients of  $8 \sim 9 \times 10^{-5} \text{ } ^\circ\text{C}/\text{m}$  (all-9209/9309 except KF in Table 1). However, the cross-frontal heat flux and the eddy diffusivity in CTF and the southern CCF/TF are roughly half those south of Cheju. This difference is attributable to finestructure characteristics in these frontal zones, strength of cross-frontal currents, and cooling-off/diluting-off extent of the Tsushima Warm Current flowing over the ECS shelf. The mixing

zone between the modified HSBCW and the Tsushima Warm Current water is rather shifted southeast in the spring than the summer, and accordingly the variance, the flux, and the diffusivity are larger in CCF/TF than south of Cheju (CCF/TF -9305 and south of Cheju -9305 in Table 1). The averaged variance and the horizontal temperature gradient are larger in the region where the Tsushima Warm Current branches from the Kuroshio than the Kuroshio region (TF branching and KF in Table 1).

Table 1. Estimates of averaged variance of vertical temperature gradient (VTG), cross-frontal temperature gradient (HTG), cross-frontal heat flux (HF), and lateral eddy diffusivity (ED) that are averaged over the each grey box (see Fig. 12 for the location). HF and ED were not estimated for the profiles in which the thermo-cline intrusion or interleaving was not prominent.

	VTG/ $^\circ\text{C}^2 \cdot \text{m}^{-2}$	HTG/ $^\circ\text{C} \cdot \text{m}^{-1}$	HF/ $^\circ\text{C} \cdot \text{m} \cdot \text{s}^{-1}$	ED/ $\text{m}^2 \cdot \text{s}^{-1}$
B1 (CTF-9209/9309)	$6.15 \times 10^{-3}$	$9.14 \times 10^{-5}$	$6.74 \times 10^{-3}$	$7.37 \times 10^1$
B1 (CTF-9305)	$2.34 \times 10^{-4}$	$6.49 \times 10^{-5}$	$3.65 \times 10^{-4}$	$5.62 \times 10^0$
B2 (south of Cheju-9209/9309)	$9.85 \times 10^{-3}$	$8.26 \times 10^{-5}$	$1.19 \times 10^{-2}$	$1.44 \times 10^2$
B2 (south of Cheju-9305)	$3.78 \times 10^{-4}$	$3.83 \times 10^{-5}$	$9.87 \times 10^{-4}$	$2.57 \times 10^1$
B3 (CCF/TF-9209/9309)	$5.07 \times 10^{-3}$	$8.35 \times 10^{-5}$	$6.07 \times 10^{-3}$	$7.27 \times 10^1$
B3 (CCF/TF-9305)	$3.10 \times 10^{-3}$	$5.11 \times 10^{-5}$	$6.07 \times 10^{-3}$	$1.19 \times 10^2$
B4 (TF branching-9209/9309)	$1.10 \times 10^{-3}$	$8.11 \times 10^{-5}$		
B4 (TF branching-9305)	$2.66 \times 10^{-4}$	$8.36 \times 10^{-5}$		
B5 (KF-9209/9309)	$3.43 \times 10^{-4}$	$4.58 \times 10^{-5}$		
B5 (KF-9305)	$2.57 \times 10^{-4}$	$3.76 \times 10^{-5}$		

As the profiles in/around TF branching and KF show irregular-staircase structures that consist of alternative sheets (strong temperature gradient in short vertical distance) and layers (almost isothermal layer in rather longer vertical distance), rather than the thermocline intrusion or interleaving (Park and Chu, 2008), the cross-frontal heat flux and the lateral eddy diffusivity were not calculated. The variance of the vertical temperature gradient  $O(10^{-4} \text{ } ^\circ\text{C}^2/\text{m}^2)$  in KF (Table 1) is around ten times lower than that elsewhere in the HES and comparable to a value of  $3 \times 10^{-4} \text{ } ^\circ\text{C}^2/\text{m}^2$  integrated from 1 to 100 m wavelength by Bao et al. (1996), which was computed at ( $28.9^\circ \text{N}$ ,  $128.2^\circ \text{E}$ ) using

spring-time observational data. They estimated the cross-frontal heat flux ( $5.5 \times 10^{-4} \text{ } ^\circ\text{C} \cdot \text{m}/\text{s}$ ) and the lateral eddy diffusivity ( $10.3 \text{ m}^2/\text{s}$ ), which are lower than those in the southern CCF tongue, TF, and CTF. In KF those two values might fall on  $O(10^{-4} \text{ } ^\circ\text{C} \cdot \text{m}/\text{s})$  and  $O(1 \sim 10 \text{ m}^2/\text{s})$ , respectively. The cross-frontal heat flux estimated here is approximated to that in the Gulf Stream, the polar front (Antarctic Circumpolar Current), the confluence zone of the North Atlantic deep water, and the circumpolar deep water, and Meddy Sharon. The lateral eddy diffusivity is approximated to that in Meddy Sharon and the Oyashio front by Ruddick and Richards (2003, Table 1).

Table 2. Estimates of averaged variance of vertical temperature gradient (VTG), cross-frontal temperature gradient (HTG), cross-frontal heat flux (HF), and lateral eddy diffusivity (ED) at stations marked with crosses and numbers in Fig. 12.

Station	9209	9305	9309
VTG/226/°C <sup>2</sup> · m <sup>-2</sup>	$2.83 \times 10^{-3}$		
HTG/226/°C · m <sup>-1</sup>	$1.00 \times 10^{-4}$		
HF/226/°C · m · s <sup>-1</sup>	$2.83 \times 10^{-3}$		
ED/226/m <sup>2</sup> · s <sup>-1</sup>	$2.83 \times 10^1$		
VTG/227/°C <sup>2</sup> · m <sup>-2</sup>	$2.77 \times 10^{-3}$		
HTG/227/°C · m <sup>-1</sup>	$1.70 \times 10^{-4}$		
HF/227/°C · m · s <sup>-1</sup>	$1.62 \times 10^{-3}$		
ED/227/m <sup>2</sup> · s <sup>-1</sup>	$9.52 \times 10^0$		
VTG/267/°C <sup>2</sup> · m <sup>-2</sup>		$8.29 \times 10^{-3}$	
HTG/267/°C · m <sup>-1</sup>		$7.96 \times 10^{-5}$	
HF/267/°C · m · s <sup>-1</sup>		$1.04 \times 10^{-2}$	
ED/267/m <sup>2</sup> · s <sup>-1</sup>		$1.31 \times 10^2$	
VTG/254/°C <sup>2</sup> · m <sup>-2</sup>		$9.31 \times 10^{-3}$	
HTG/254/°C · m <sup>-1</sup>		$1.02 \times 10^{-4}$	
HF/254/°C · m · s <sup>-1</sup>		$9.16 \times 10^{-3}$	
ED/254/m <sup>2</sup> · s <sup>-1</sup>		$9.01 \times 10^1$	
VTG/217/°C <sup>2</sup> · m <sup>-2</sup>			$2.12 \times 10^{-2}$
HTG/217/°C · m <sup>-1</sup>			$8.65 \times 10^{-5}$
HF/217/°C · m · s <sup>-1</sup>			$2.45 \times 10^{-2}$
ED/217/m <sup>2</sup> · s <sup>-1</sup>			$2.84 \times 10^2$
VTG/228/°C <sup>2</sup> · m <sup>-2</sup>		$8.04 \times 10^{-4}$	$3.77 \times 10^{-3}$
HTG/228/°C · m <sup>-1</sup>		$2.62 \times 10^{-5}$	$1.46 \times 10^{-4}$
HF/228/°C · m · s <sup>-1</sup>		$3.07 \times 10^{-3}$	$2.58 \times 10^{-3}$
ED/228/m <sup>2</sup> · s <sup>-1</sup>		$1.72 \times 10^2$	$1.76 \times 10^1$
VTG/255/°C <sup>2</sup> · m <sup>-2</sup>		$4.36 \times 10^{-4}$	$9.46 \times 10^{-4}$
HTG/255/°C · m <sup>-1</sup>		$4.80 \times 10^{-5}$	$2.30 \times 10^{-4}$
HF/255/°C · m · s <sup>-1</sup>		$9.02 \times 10^{-4}$	$4.12 \times 10^{-4}$
ED/255/m <sup>2</sup> · s <sup>-1</sup>		$1.89 \times 10^1$	$1.79 \times 10^0$

The cross-frontal heat flux and the lateral eddy diffusivity tend to be larger at the shoreward side of the southern CCF/TF than at the center of it (Sta. 226 > Sta. 227, Sta. 267 > Sta. 254 in Table 2), because the variance of the vertical temperature gradient is comparable at both stations but the cross-frontal temperature gradient is stronger on the center of the front. The larger flux and diffusivity are due to the frequent occurrence of thermocline intrusion or interleaving at the shoreward side of the front; the

frontal exchange occurs more vigorously at the shoreward side of the front since the water mass at shoreward side takes a leading role in variability of the front (PC06). In the summer, the cross-frontal heat flux and the lateral eddy diffusivity tend to be slightly larger in the northern part than the southern part of the front (Sta. 217 > Sta. 228 > Sta. 255 in Table 2 – 9309), implying that the degree of cross frontal exchange would be different along the front.

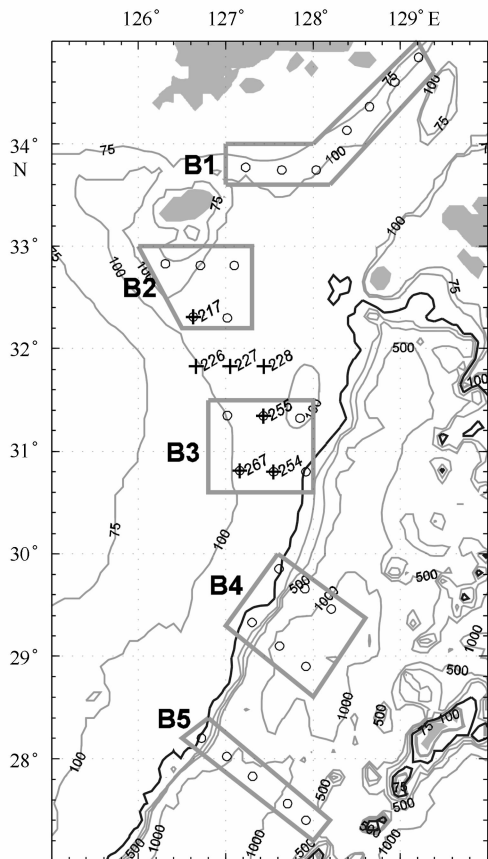


Fig. 12. AXBT stations for calculating vertically-averaged variance of vertical temperature gradient, cross-frontal temperature gradient, heat flux, and eddy diffusivity. Five grey boxes are labeled by B1 (CTF), B2 (south of Cheju), B3 (CCF/TF), B4 (TF branching), and B5 (KF). Box-averaged estimates of the four parameters are listed in Table 1, and estimates of the parameters for individual stations marked with crosses and numbers in Table 2.

## 6 Conclusions

We have examined the synoptic features in/around the thermal fronts and cross-frontal heat flux in the southern Huanghai Sea and the East China Sea using four AXBT surveys in 1992 and 1993 and presented the plausible interpretations of them. The thermal fronts described by PC06 were detected as well

using these data: Cheju-Changjiang front, Cheju-Tsushima front, Tsushima front, and Kuroshio front. In addition, detailed features in/around the thermal fronts, which were not seen in PC06, were discovered. The new results from this study are summarized as follows.

(1) The southern CCF tongue has a variety of features in warm seasons: multiple cold mass boundaries, mergence of the thermal front by the Taiwan Warm Current on the ECS shelf, and poor (rich) thermocline intrusion around its western (eastern) part by strong summer bottom tidal mixing. In the spring of 1993, a frontal eddy-like feature with a horizontal scale of approximately 100 km is detected in TF. In the summer of 1993, the homogeneous water of approximately 18°C splits the combined front of CCF and TF locally in the horizontal view and infiltrates into the thermocline in 127° ~ 128° E in the vertical view.

(2) The cyclonic meandering of CTF is sustained throughout the season regardless of its spatio-temporal variability and related to the near-bottom cold water of 14 ~ 16°C. In the summer the inverted structures, i. e., warm-anomaly, at the bottom of the surface mixed layer (10 ~ 50 m depth) are detected in CTF with the thickness of ~ 10 m and the temperature range of about 0.5 ~ 1°C warmer than surroundings. The downward heat flux by anticyclonic motion might cause this phenomenon.

(3) The multistructure of KF is distinct when the warm eddies along the Okinawa Trench are developed, whereas the inner KF exists throughout the year.

(4) The cross-frontal heat flux is not equivalent among the HES fronts because of differences in surrounding water masses and finestructure characteristics, even though the HES fronts are related with each other through the connected current system in the HES. In KF the variance of the vertical temperature gradient is  $O(10^{-4} \text{ } ^\circ\text{C}^2/\text{m}^2)$ , which is around ten times lower than elsewhere in the HES. In warm

seasons the cross-frontal heat flux and the lateral eddy diffusivity are the largest [ $O(10^{-2} \text{ } ^\circ\text{C} \cdot \text{m/s})$  and  $O(10^2 \text{ m}^2/\text{s})$ , respectively] in the mixing zone between the modified HSBCW and the Tsushima Warm Current, which is formed south of Cheju in the summer but rather shifted southeast in the spring (than summer). The sharp contrast between the two water masses and the vertically-sheared advection might be responsible for this large exchange of heat.

(5) The summer connected CCF/TF and CTF reveals roughly equal cross-frontal temperature gradient, but different cross-frontal heat exchanges. The cross-frontal heat exchange is lower in CTF, implying differences of frontal finestructures. The cross-frontal heat flux and the lateral eddy diffusivity tend to be larger on the shoreward side than at the center of the southern CCF/TF, caused by the frequent occurrence of thermocline intrusion or interleaving on the shoreward side of the front.

## References

Bao X W, Fang X H, Liu X G. 1996. Thermohaline fine-structure and its relation with the water masses and currents system in the northern East China Sea. *Chinese J of Oceanol and Limnol*, 14(2):122 ~ 128

Boyd J D, Linzell R S. 1993. Evaluation of the Sparton tight-tolerance AXBT. *J Atmos Oceanic Technol*, 10: 892 ~ 899

Boyer T P, Levitus S. 1994. Quality control and processing of historical temperature, salinity, and oxygen data. NOAA Technical Report NESDIS 81

Chen C, Beardsley R, Limeburner R, et al. 1994. Comparison of winter and summer hydrographic observations in the Yellow and East China Seas and adjacent Kuroshio during 1986. *Cont Shelf Res*, 14:909 ~ 929

Chu P C, Chen Y C, Kuninaka A. 2005. Seasonal variability of the East China/Yellow Sea surface buoyancy flux and thermohaline structure. *Adv Atmos Sci*, 22: 1 ~ 20

Chu P C, Fan C W, Lozano C J, et al. 1998. An airborne expandable bathythermograph survey of the South China Sea, May 1995. *J Geophys Res*, 103:21637 ~ 21652

Chu P C, Fralick C R, Haeger S D, et al. 1997. A parametric

model for Yellow Sea thermal variability. *J Geophys Res*, 102(C3):10499 ~ 10508

Chu P C, Wells S K, Haeger S D, et al. 1997. Temporal and spatial scales of the Yellow Sea thermal variability. *J Geophys Res*, 102(C3): 5655 ~ 5668

Du Y, Qi Y, Chen J, et al. 2003. Sea current observation during ASIAEX East China Sea planning. *Ocean Engineering* (in Chinese), 21(1): 94 ~ 100

Furey H, Bower A. 2005. The synoptic temperature structure of the East China and southeastern Japan/East Seas. *Deep Sea Res(II)*, 52: 1421 ~ 1442

Garrett C. 1979. Mixing in the ocean interior. *Dyn Atmos Oceans*, 3: 239 ~ 265

Georgi D T. 1981. On the relationship between the large-scale property variations and fine structure in the circumpolar deep water. *J Geophys Res*, 86: 6556 ~ 6566

Guo B, Lie H J, Lee J H. 1998. Interaction of the Kuroshio and shelf water in the Tsushima Warm Current region in summer. *Acta Oceanologica Sinica*, 20(5):1 ~ 12

Hickox R, Belkin I M, Cornillon P, et al. 2000. Climatology and seasonal variability of ocean fronts in the East China, Yellow and Bohai Seas from satellite SST data. *Geophys Res Lett*, 27(18):2945 ~ 2948

Hsu M K, Mitnik L M, Hu J H, et al. 1997. Kuroshio front and oceanic phenomena near Taiwan on ERS SAR images. *Proceeding of the 3rd ERS Symposium: Space at the Service of our Environment*. Florence: 17 ~ 21

Hu D X. 1994. Some striking features of circulation in Huanghai Sea and East China Sea. In *Oceanology of China Seas*. Zhou D, Liang Y B, Tseng C K, tds. Netherlands: Kluwer Academic Publishers, 27 ~ 38

Hur H B, Jacobs G A, Teague W J. 1999. Monthly variations of water masses in the Yellow and East China Seas. *J Oceanogr*, 55(2):171 ~ 184

Ichikawa H, Beardsley R C. 2002. Review: the current system in the Yellow and East China Seas. *J Oceanogr*, 58(1):77 ~ 92

Isobe A. 1999. The Taiwan-Tsushima Warm Current system: its path and the transformation of the water mass in the East China Sea. *J Oceanogr*, 55(2):185 ~ 195

Isobe, Fujiwara A E, Chang P H, et al. 2004. Intrusion of less saline shelf water into the Kuroshio subsurface layer in the East China Sea. *J Oceanogr*, 60(5):853 ~ 863

James, Wimbush C M, Ichikawa H. 1999. Kuroshio meanders

- in the East China Sea. *J Phys Oceanogr*, 29:259 ~ 272
- Joyce T M. 1977. A note on the lateral mixing of water masses. *J of Phys Oceanogr*, 7: 626 ~ 629
- Jugan M J, Beresford H. 1992. Editing approach for the Navy's Master Oceanographic Observation Data Set. *Proceedings of MTS '91, An Ocean Cooperative: Industry, Government, and Academia*. 1164
- Kim H J, Yug S S. 1983. Inversion phenomena of temperature in the Southern Sea of Korea. *Bull Korean Fish Soc (in Korean)*, 16(2):111 ~ 116
- Kondo M. 1985. Oceanographic investigations of fishing grounds in the East China Sea and the Yellow Sea—I. Characteristics of the mean temperature and salinity distributions measured at 50 m and near the bottom. *Bull of Seikai Region Fish Res Lab (in Japanese)*, 62:19 ~ 55
- Lee J H, Lie H J, Cho C H. 2003. The structure of ocean fronts in the East China Sea. *Proceedings of the 12th PAMS/JECSS Workshop*. 2 - 10 - 1 ~ 2
- Lee J C, Na J Y, Chang S D. 1984. Thermohaline structure of the shelf front in the Korea Strait in early winter. *J Korean Soc Oceanogr*, 19(1):56 ~ 67
- Lie H J, Cho C H, Lee J H, et al. 2000. Seasonal variation of the Cheju Warm Current in the northern East China Sea. *J Oceanogr*, 56(2):197 ~ 211
- Ning X, Liu Z, Cai Y, et al. 1998. Physicobiological oceanographic remote sensing of the East China Sea: satellite and in situ observations. *J Geophys Res*, 103(C10):21623 ~ 21635
- Oka E, Kawabe M. 1998. Characteristics of variations of water properties and density structure around the Kuroshio in the East China Sea. *J Oceanogr*, 54: 605 ~ 617
- Park Y H. 1986. Water characteristics and movements of the Yellow Sea Warm Current in summer. *Prog in Oceanogr*, 17: 243 ~ 254
- Park S, Chu P C. 2008. Characteristics of thermal fine structures in the southern Yellow and East China Seas from airborne expendable bathythermograph measurements. *J Oceanogr*, in press
- Park S, Chu P C. 2006a. Interannual SST variability in the Japan/East Sea and relationship with environmental variables. *J Oceanogr*, 62(2): 115 ~ 132
- Park S, Chu P C. 2006b. Thermal and haline fronts in the Yellow/East China Seas: surface and subsurface seasonality comparison. *J Oceanogr*, 62(5):617 ~ 638
- Park S, Chu P C. 2007. Synoptic distributions of thermal surface mixed layer and thermocline in the southern Yellow and East China Seas. *J Oceanogr*, 63(6):1021 ~ 1028
- Qui B, Toda T, Imasato N. 1990. On Kuroshio front fluctuations in the East China Sea using satellite and in situ observational data. *J of Geophys Res*, 95(C10):18191 ~ 18204
- Ruddick B, Richards K. 2003. Oceanic thermohaline intrusions: observations. *Prog in Oceanogr*, 56: 499 ~ 527
- Son Y T, Lee S H, Lee J C, et al. 2003. Water masses and frontal structures in winter in the northern East China Sea. *J of Korean Soc of Oceanogr (The Sea) (in Korean)*, 8(3):327 ~ 339
- Tang Y, Zou E, Lie H J, et al. 2000. Some feature of circulation in the southern Huanghai Sea. *Acta Oceanologica Sinica*, 22(1):1 ~ 16
- Wang D, Liu Y, Qi Y, et al. 2001. Seasonal variability of thermal fronts in the northern South China Sea from satellite data. *Geophys Res Lett*, 28: 3963 ~ 3966
- Yanagi T, Shimizu T, Lie H J. 1998. Detailed structure of the Kuroshio frontal eddy along the shelf edge of the East China Sea. *Cont Shelf Res*, 18: 1039 ~ 1056
- Yoo S H, Ho C H, Yang S, et al. 2004. Influences of tropical-western and extratropical Pacific SSTs on the East and Southeast Asian climate in the summers of 1993 - 94. *J Climate*, 17(13):2673 ~ 2687